Highlights of Borehole Imaging, Tauhara Geothermal Field Drilling, New Zealand

Cécile Massiot[1], Sarah D Milicich[1], Fabian Sepulveda[2*], Matthew J Sophy[2], Mark JF Lawrence[1], Angela G Griffin[1], Mike Rickman[3], Lucy B Carson[4], Michael Rosenberg[4], Mark Simpson[4]

[1]GNS Science, Avalon Research Center, 1 Fairway Drive, Avalon 5010, New Zealand.

[2]Contact Energy, 3352 State Highway 1, Wairakei, Taupō 3352, New Zealand (*now at: Mercury New Zealand Limited, 283 Vaughan Rd, Owhata, Rotorua 3010, New Zealand)

[3]HADES, Tauranga, New Zealand

[4]GNS Science, 114 Karetoto Road, RD4, Taupō 3384, New Zealand

c.massiot@gns.cri.nz

Keywords: *well targeting, conceptual model, borehole image, structural permeability, Tauhara Geothermal Field, New Zealand.*

ABSTRACT

Assessing fracture characteristics is key to robust assessment of the contribution of structural permeability to a well's capacity for production or injection. Contact Energy acquired eleven borehole images at the Tauhara Geothermal Field, New Zealand, during the 2011, 2019 and 2021-2022 drilling campaigns. Here, we present some key observations from borehole imaging at Tauhara. The borehole imaging technology adopted in the 2021-2022 Tauhara drilling program was the Acoustic Borehole Imager (ABI43) from ALT provided through HADES and MB Century in New Zealand. The ABI43 imaging sensor is rated to 170°C and the orientation sensor to 125°C. The ABI43 tool was run down into formation temperatures in the range of 200-300°C, with well quenching keeping temperatures generally <125°C. Borehole images provided measurements of: 1) fracture appearance, density, orientation, and apparent thickness, and 2) in-situ stress orientations. Borehole image interpretations were then combined with geological interpretation of drill cuttings and permeable (feed) zones delineated using downhole measurements of pressure, temperature and spinner velocity (PTS). The combined datasets were interpreted to evaluate the nature of permeability and characterise the fracture network including potential fault intersections in the boreholes. The data also aided interpreting hydrothermally altered lithology types and unit boundaries.

Reservoir-scale faults were interpreted from the images and major feed zones were often found associated with these reservoir-scale faults, or with fracture clusters. Minor feed zones were usually associated with fracture clusters or fractures spread out over a larger interval. In some minor feed zones, lack of fractures suggests that fluid flow is not clearly controlled by local fractures. Integration of borehole images with geological and reservoir measurements revealed that permeability is heavily controlled by fractures at the new production and injection areas of Tauhara. This observation had implications for well targeting strategies during the drilling campaign and the geothermal system conceptual model.

1. INTRODUCTION

Fractures and faults are a key contributor to permeability in many geothermal fields (e.g., Davatzes & Hickman, 2010; Jolie et al., 2021 and references therein). While it is possible to interpret dominant strike of geological structures in normal stress regime settings such as in the Taupō Volcanic Zone (TVZ), outcrop analogue, geophysical and geochemical surveys are insufficient to identify and predict the specific location, dip magnitude and dip direction of permeable structures at reservoir depth prior to drilling. Borehole imaging data can fill gaps in information and progressively improve our ability to define areas of enhanced structural permeability for well targeting.

Borehole images provide oriented "pictures" of the inside wall of boreholes. Borehole image analysis provides measurements of fracture location (hence density along the well), appearance, orientation and apparent thickness; and determination of in-situ stress directions from drilling-induced features. Borehole images can also complement stratigraphic and lithological information from drill cutting analysis, and in some instances, may represent the only source of geological information (e.g., in lost circulation zones). Coring, while valuable, is expensive and provides limited spatial coverage of the reservoir of fracture orientation (apparent dip magnitude only, dip direction not available).

Here, we present some general observations from borehole images acquired in wells of the Tauhara Geothermal Field, Aotearoa New Zealand, obtained during 2011, 2019 and 2021-2022 drilling campaigns. Four borehole images from the 2021-2022 development program are used to demonstrate some key findings in the new areas of production and injection. We also discuss implications of borehole image interpretations to the conceptual model of the geothermal field and how this evolving concept model was used to refine and fine-tune drilling targets.

1.1 Tauhara, Pre-campaign Conceptual Model

The Tauhara and Wairakei Fields comprise the Wairakei-Tauhara geothermal system, located near Taupō (Figure 1). Although each area has distinct upflow zones, direct pressure communication has been documented across Wairakei-Tauhara (McDowell et al., 2020). This fact combined with numerical modelling insights largely supported the concept model of formational permeability being extensive across Wairakei-Tauhara.

The Wairakei-Tauhara geothermal system has a surface area of 124 km2 (within a 100 ohm.m electrical resistivity contour), about two-thirds of which represents the Tauhara Field. Volcanic and sedimentary rocks have accumulated for <1.6 Ma overlying a basement (>2500 m deep at Tauhara) of Mesozoic (>125 Ma) greywacke (Rosenberg et al., 2020). In the Tauhara Field, volcanic rocks at production and injection depths are dominantly rhyolitic welded and non-welded

ISSN 2703-4275

tuffs, and lavas. The production and reinjection reservoir are capped by relatively low permeability lacustrine siltstone-sandstone formations.

The structural fabric of the Tauhara Field, as revealed by surface active faults mapping and drilling is the local expression of the broader Taupō Rift (Villamor et al., 2017). Extension in the Taupō Rift coincides with the southern, onshore part of the Hikurangi subduction zone's volcanic arc (i.e., the TVZ) and is thus referred to as an intra-arc rift. The Taupō Rift is dominated by northeast-southwest trending normal faults (Rowland and Sibson, 2001; New Zealand Active Faults Database 2003–; Villamor et al., 2017). In addition to fractures induced by faulting, some fractures are very likely to be joint sets related to cooling contraction after pyroclastic or lava flow emplacement.

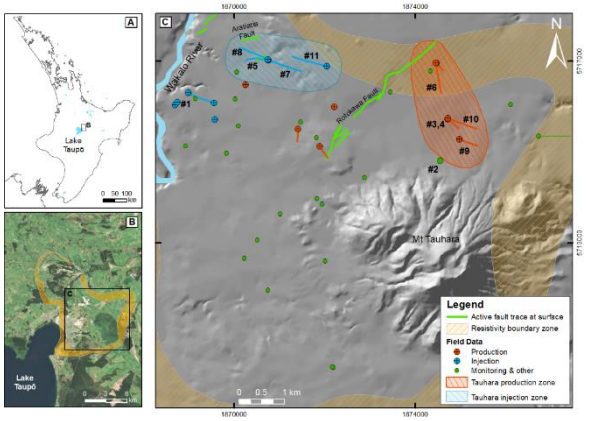

Figure 1: Map of the Tauhara Geothermal Field. A): Location of the Tauhara Geothermal Field in the North Island of New Zealand. B) location of the map area in C) with the resistivity boundary of the Wairakei-Tauhara Geothermal Field (Risk et al., 1984). C) Map of the area of the Tauhara Geothermal Field highlighting new production and injection areas (to be commissioned in 2023) and wells where borehole images were acquired between 2011-2021. Base map: 8 m shade model. Active faults: New Zealand Active Faults Database (2003–). The numbering corresponds to sampling locations for well data (borehole images, PTS logs, etc.) in the order of data collection during the drilling and logging campaign.

1.2 Tauhara Field development history

Early exploration of Tauhara took place in the 1960s and 1970s (mainly Tauhara North and Tauhara Central areas) providing first confirmation of a high-temperature (250-280°C) geothermal resource. A second phase of appraisal drilling was completed during 2006-2012 confirming reservoir temperatures in the range of 250°C- >300°C across Tauhara North, East, Central and South, with the top of the reservoir being as deep as ca. 900 m below ground level in the east part of Tauhara (further details of Tauhara development history in McDowell et al., 2020).

In 2019, Contact Energy commenced a new appraisal drilling program focused on the Tauhara East area. The purpose of this program was to delineate the extent of the Tauhara East high-temperature reservoir (four vertical wells drilled) and inform the field development strategy, specifically regarding the location of injection. During this phase of drilling, three new borehole images were acquired from two wells (in the production section of both wells and, in one of these two wells, also in the section of the hole that is cased after borehole imaging). Appraisal drilling and borehole imaging identified areas of high temperature but low permeability in the southern margin of the known productive reservoir. These areas also exhibited contrasting geology and structural orientations (oblique to the Taupō Rift fabric) challenging the concept model of purely formational, laterally-extensive permeability. In the northern part of the known productive reservoir, new wells intersected high-enthalpy fluids in a highly permeable reservoir.

In 2020, with financial approval granted for a 168 MWe geothermal project, Contact Energy commenced a production and injection drilling program, focused on Tauhara East for production and Tauhara North for injection. Following recognition that permeability was significantly influenced by fractures, all new wells (seven) were designed to be directional and borehole imaging in production sections was adopted as a routine well evaluation technique. Borehole imaging proceeded relatively smoothly with a few exceptions where logging was limited or suspended due to a combination of high formation temperature, high permeability and/or formation instability. While Contact Energy's drilling program was based on multiple-well pads, wells from the same well pad were not drilled consecutively but separated in time. This afforded the time for well evaluation, including data acquisition and data interpretation. More importantly, this allowed for subsequent well targeting to be based on all available information, which was a key contributor to the success of the drilling program in general and borehole imaging program in particular.

1.3 Borehole Imaging in Geothermal Field Developments: Brief Overview

Borehole image interpretation allows the detection of fabrics and structures intersected by the borehole (e.g., fractures, veins, layering) together with their orientation and morphological characteristics; stress-induced features when present; and indications of the rock types. Borehole images provide high-resolution images (i.e., a vertical resolution of 5-10 mm) of the borehole wall surface, oriented to geographic north. There are three types of borehole imaging technologies. Ultrasonic ('acoustic') images of the borehole surface, commonly called borehole TeleViewer (BHTV) logs, are generated by measuring the travel time and impedance of ultrasonic pulses sent and received by a piezoelectric transducer (Poppelreiter et al., 2010; Zemanek et al., 1970). The ultrasonic sensor does not require direct contact with the rock formation. Electrical microresistivity images show contrasts in resistivity at the borehole wall via four pads with electrodes in contact with the borehole wall. Optical imaging tools use similar principles as cameras, however they are not used in deep geothermal wells because they require optically transparent fluid (more crucial in large bore geothermal wells than slim exploration wells) and are limited by low operating temperature. Microresistivity images tend to show more lithological details while acoustic images tend to highlight the fractures most likely to be permeable (Davatzes and Hickman, 2010).

Borehole imaging is increasingly used in geothermal fields worldwide to assess the structural settings and identify characteristics of permeable fractures (e.g., Barton and Zoback, 1992; Genter et al., 1997; Davatzes and Hickman, 2010; Masri et al., 2015; Vidal and Genter, 2018; Millet et al., 2020; Mutonga and Yasuhiro 2021).

ISSN 2703-4275

In New Zealand geothermal fields, borehole images revealed the local structural settings, links to permeable zones and some lithological constraints at the Wairakei (Massiot et al., 2017a; McNamara et al., 2019; Massiot et al., 2020; Milicich et al., 2021), Ngatamariki (Halwa et al., 2013), Kawerau (Wallis et al., 2012), and Rotokawa (McNamara et al., 2015; Massiot et al., 2017b). At Wairakei, those previous studies found that only a portion of the structures identified on borehole images supply geothermal fluids. Fractures in permeable zones are typically 1) of low amplitude and seen on the travel-time image of acoustic images; or 2) are low-resistivity fractures with high-resistivity haloes on resistivity images. In addition, permeable zones preferentially contain high fracture density and wide aperture fractures. However, similar fracture characteristics were also observed outside permeable zones, which implies that factors such as hydrothermal mineral sealing and/or connectivity to the reservoir-scale fracture network affect permeability in a borehole.

2. METHOD

2.1 Borehole Imaging Tool Specifications

At the Tauhara Geothermal Field, an acoustic borehole image was acquired by Tiger Energy Services in 2011 with the QL85 ABI tool (also colloquially called "AFIT" tool at that time) rated to 300°C. One resistivity borehole image was acquired in 2019 with the Formation Imager Micro Imager (FMI) tool developed and operated by Schlumberger. The FMI tool is rated to 175°C. The FMI sensors are in contact with the rock so may be more susceptible to failure near the temperature rating than acoustic imaging tools where sensors are only in contact with borehole fluids.

The acoustic borehole imaging tool used in wells drilled at Tauhara in 2019 and 2021-2022 was a QL43 ABI 2G tool prototype developed by Advanced Logic Technologies (ALT) and acquired by HADES (Figure 2). This version of the QL43 ABI 2G has a rated maximum temperature of 170°C, except for the orientation sensor measurement which is only rated to 125°C. Thus, at some point above 125°C the image will be acquired but without being orientated. Orientation sensors restart when sufficiently cooled.

This paper presents results from the 7.35 km of acoustic borehole images acquired in 8 wells since 2019 with the QL43 ABI tool, with focus on images collected in four wells during 2021 in new production and injection areas.

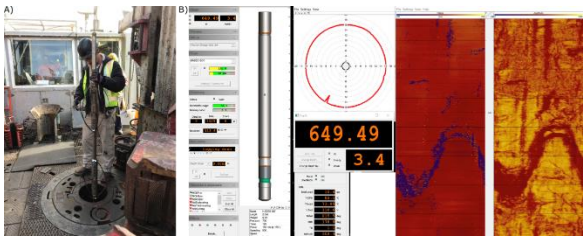

Figure 2: Acoustic borehole image acquisition. A) ABI43 tool pulled out of the well after logging. B) Screen during acquisition showing un-processed images while logging at well at location #3. Observations during logging provide first indications of borehole shape and potential fracture occurrence, though fractures are not necessarily permeable (see Section 3.2).

2.2 Acquisition

Borehole imaging services were provided by HADES (imaging tool) and MB Century (wireline operations). Borehole images were acquired after the drilling had reached terminal depth (TD) and immediately prior to running liner in the hole. Several tests can be performed to assess hole conditions prior to borehole image logging: the need for tests, and the type of tests to be performed, depends on information available at the time and the quality requirements. At Tauhara, in order to de-risk the borehole image logging operation and pre-identify areas of interest, pressure-temperature-spinner (PTS) or XY caliper were run to assess borehole temperature under injection, permeability (spinner fluid velocity) and stability (XY shape used as a proxy). During borehole image acquisition, cold water was pumped throughout image acquisition at rates up to 3800 litres per minute to keep wellbore temperatures within the operational range of the ABI tool without causing the tool to vibrate or create an air bubble in the liquid column. Logging speeds, image resolution and logging depth intervals were decided for each well based on image quality requirements, understanding of hole conditions, pre-identified areas of interest, and a pre-set cap on logging time (logging engineer fatigue management). Predetermined permeable zones were logged at a slower speed to obtain highest resolution whilst non permeable sections of the wellbore were logged at higher speeds. Eight of the nine borehole images were acquired in 12.25 inch borehole diameters; one was acquired in a 16 inch borehole diameter. Borehole deviation near TD varied between 28° and 42° from vertical.

Borehole image runs acquired images over 93% (up to 100%) of the entire open hole section in 6 of the 9 image log runs (Figure 3). This high coverage showed that tool's temperature limit (170°C) is manageable through well quenching even when in presence of high undisturbed reservoir temperature (270-300°C in the production area; 230-250°C in the injection area). The ability to quench a well may be limited by the availability of permeability. Generally, open hole temperature was hard to manage below sections of high permeability. In these cases, acquisition generally stopped immediately past the areas of interest and before reaching TD. Coverage was partial in some wells due to either high temperature, an obstruction in the well hit by both the imaging and PTS tools, or open hole stability concerns.

The orientation sensor temperature limitation (125°C) was exceeded for only 3.5% of the imaged intervals for all but one survey. In one well, only 7% of the image was oriented due to a hot inflow below the casing shoe (>125°C). In this well, unoriented images were successfully acquired in the remaining 1300 m of open hole by keeping borehole temperature under 170°C using up to 3800 litres per minute of drilling fluids. The decision to proceed with logging at temperatures between 125-170°C was based on the fact that the open-hole section was directional (>10° inclination) and that drilling pipe marks would be available to guide image re-orientation (see Section 2.4).

In one well, pump rates increased to 3000 litres per minute to keep borehole temperatures at depth below tool limitations, however this produced an air bubble at 1380 m with a liquid column above extending into the production casing. Acoustic imaging tools cannot operate outside the liquid column. By reducing the pump rates to 1000 litres per minute, the wellbore liquid column displaced the bubble and logging was continued.

ISSN 2703-4275

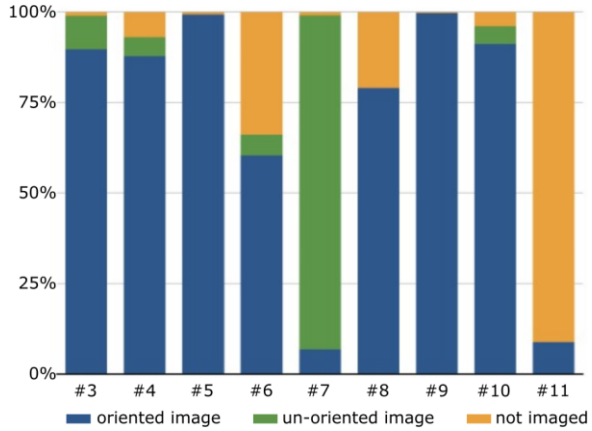

Figure 3: Proportion of open-hole sections at Tauhara imaged post-2019 with the QL43 ABI 2G acoustic borehole imaging tool. Green portions show the proportion of un-oriented image (i.e., temperature while logging between 125°C and 170°C). Well references as in Figure 1.

2.3 Image processing and analysis

The raw image data from borehole images acquired at the Tauhara Geothermal Field were exported in LIS format from the WellCAD™ file generated during acquisition for loading into Recall™ software for image processing and interpretation. A depth-based plot of the raw image curves is first produced to ensure all the required curves are present, assess raw data quality, and highlight potential processing or interpretation issues. Static and dynamic image normalisations illustrate the gross acoustic amplitude and travel time variations throughout the imaged interval, or at metre-scale, respectively (Rider 1996, Hansen & Buczak 2010). Images are displayed unwrapped images 0° (geographic N) at the left-hand edge, 180° (geographic S) in the centre and 360° (geographic N) at the right-hand edge. All feature orientations are with reference to geographic north and horizontal plane, i.e., borehole deviation and magnetic declinations have been considered.

Acoustic image quality is predominately dependent on having a perpendicular surface to reflect the acoustic energy back to the tool. Image quality is best where the tool is centralised and the borehole is circular with a smooth wall. In these mostly deviated wells, and especially in intervals where the inclination increases ("build" section), drill pipe wear on both the high and low sides result in unsymmetrical cross sectional borehole shapes.

Overall, image quality varies between and within wells with large sections of moderate (>50% image can be interpreted) to good (>75% image can be interpreted) where fracture density estimates are reliable. Decreased image quality is generally due to drilling causing drill pipe wear, spiral hole, stabiliser marks, spalling from borehole wall over large sections, or local (<5 m-long) excavations in intensely fractured or washout zones visible on the image. Stick-and-pull artefacts due to variable logging speed occur but are generally not detrimental to fracture identification. Other artefacts (Loft and Bourke, 1999) are carefully noted to avoid misinterpretation of natural or stress-induced features. Image quality acquired with the ABI43 across all new Tauhara wells is generally better than those acquired with the lower-resolution high-temperature ABI85 at Wairakei (McNamara et al., 2019).

Fractures, layers and in-situ stress features are manually fitted to features on the image in Recall™ software (after Rider 1996). Dip types are classified as presented in Massiot et al. (2015). Low-acoustic amplitude fractures are the most common type of fractures and can be interpreted as either 1) open fractures filled with drilling fluid (hence permeable); 2) closed fractures filled with clay or sulfide minerals or 3) any combination of the above (open, closed, or partially open). Fractures of low acoustic amplitude that are also observed on the travel-time image are the most likely to be permeable (Massiot et al., 2017a; McNamara et al., 2019). In hydrothermal settings, option 3 above is most applicable. Therefore, additional information is required to determine if fractures are open with potential to support fluid flow.

2.4 Re-orientation of image intervals that lack orientation sensors

In some image intervals in some wells, borehole fluid temperature exceeded the orientation sensor tolerance (>125°C) but an image was still acquired up to 170° C. In these intervals, the feature appearance and density are reliable, but the orientation is not. The following procedure was conducted in well at location #7 to provide possible, low certainty constraints on feature orientations using the low-side furrow (LSF) and high-side furrow (HSF) drilling marks visible in the image (Figure 4). The LSF and HSF orientations were found to consistently occur throughout the oriented interval of the borehole. An independent survey of well deviation indicated that the borehole deviation was constant (inclination and azimuth). In the unoriented part of the image the LSF and HSF were rotated back to match the consistently oriented LSF and HSF above (Figure 4) in an iterative process that continued until an optimum orientation was achieved. This re-orientation assumes the LSF is always at the low-side of the borehole and in a deviated borehole the low-side will maintain a consistent orientation in the unoriented section of the borehole. However:

1. The LSF may not always be exactly at the low-side of the borehole because the drill bit can "climb" as it rotates. This may be due to factors such as the rate of bit rotation, rate of penetration, weight on bit etc. In this study, comparison in nearby wells where the images were oriented showed that in 50% cases, furrows are about 30° apart from high/low side. As a broad approximation, subtracting 30° from the mean fracture strike (i.e., rotating counterclockwise) may provide a better estimate of mean fracture orientations.
2. The LSF and HSF are not perfectly linear features (Figure 4) and orientations can vary over small intervals (metre-scale). As the measured LSF/HSF orientations are averages of a metre to a few metres, not all the variability was captured and may have introduced some extra uncertainty into the final image orientation, particularly where tool rotation during acquisition is significant and highly variable.

In summary, this procedure increases the value of images collected in intervals where temperature is 125°C -170°C by adding some constraints on feature orientation to their reliable density and appearance.

ISSN 2703-4275

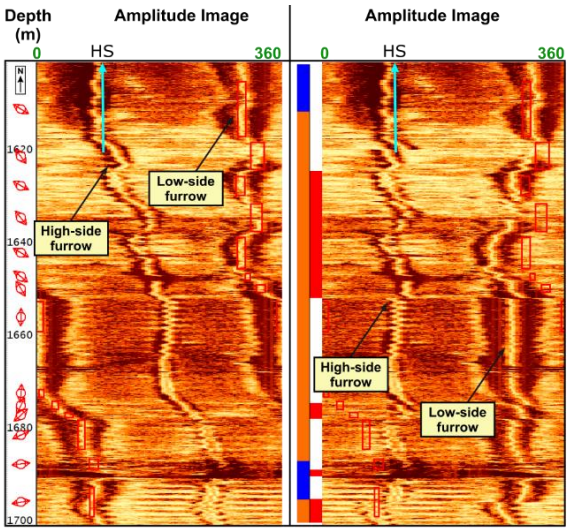

Figure 4: Image reorientation when temperature exceeds orientation sensors limits (125°C), well #7. Left) Amplitude image from the interval 1600–1700 mRF (metres below rig floor) where orientation sensors were not working. Image tool rotation is indicated by the low-side orientation (red rectangles and mean orientations). Right) Same interval with the image re-oriented so the low-side furrow maintains a consistent orientation to the low side of the borehole. Red rectangles: unrotated position of the LSF. Coloured bars to the left of the image: image quality (left) and intervals of highest orientation uncertainty in red (right). Blue arrow at the top of each image: orientation of the borehole high side (HS).

2.4 Integrated analysis of geology, borehole images and PTS logs

The PTS interpretation method is described in detail in Massiot et al. (2017a) and used by McNamara et al. (2019) for the Wairakei Geothermal Field. The method combines (1) changes in temperature gradient during injection, (2) changes in temperature gradient during heat up, (3) steps in fluid velocity profiles from spinner data, (4) steps in the ratio of fluid velocity profiles from different injection rates, and (5) observation of the pressure control point during heat up. Permeable zones are classified as "major" when multiple indicators are clearly observed, thus indicating a higher contribution to fluid flow in the borehole and rated "medium" or "minor" otherwise. The interpretation of the location and extent of permeable zones is subsequently refined by a joint interpretation of PTS and borehole image results, which improves the coarse resolution and uncertainty of interpretation of PTS data alone (Massiot et al., 2017a).

At Tauhara, the interpretation workflow was similar to that presented in Massiot et al. (2017a) but at a faster pace and with interpretation focusing on key information needed to support well targeting. Borehole images were interpreted within two weeks after borehole image acquisition. During this time, discussions with geologists who describe cuttings ensure image interpretation is consistent with geological interpretation of lithology, potential fractured zones and fracture fill. PTS logs and preliminary interpretation of permeable zones were provided by reservoir engineers to borehole image analysts after 7-10 days to produce summary figures. A presentation of results at the end of these two weeks allowed for rapid and efficient sharing of key outcomes of structural analysis (especially fracture location and orientation) and implications for permeability, with considerations of drilling events and nuances in delineating preliminary feed zones. Information from borehole images could then be used to aid targeting the next well, while the borehole image analysts finalised the report with the extra drilling and reservoir engineering information.

3. STRUCTURES AND PERMEABILITY

3.1 Breccia image patterns

A "brecciated" image pattern occurs in several wells, sometimes at several depths within a well. This pattern appears as multiple, closely-spaced, 1-10 cm-large patches of low acoustic amplitude and/or loss signal, hence appearing on the travel-time image (Figure 5). This pattern is generally observed together with fractures seen on the travel-time image, and sometimes confined between two fractures seen on the travel-time image. Some brecciated image patterns are not well-developed and are noted as such during image interpretation.

Breccias in volcanic rocks can be structural (fault breccia) or lithological (inherent to their mode of formation). In addition, drilling artefacts that would cause spalling (rock fragments broken off from the borehole wall) need to be carefully considered before interpreting these patterns as natural, especially between fractures seen on travel-time image where natural spalling is confined within the fracture. As a guideline, brecciated patterns that occur in the same depth interval as fractures seen on the travel-time image are considered as potential fault breccia. Further consideration of the presence of nearby faults from a 3-D geological model, local stress rotations (interpreted from drilling-induced tensile fractures) and/or occurrence in permeable zones delineated from PTS logs, can validate that interpretation of fault breccia.

3.2 Characteristics of fractures within and outside permeable zones: example of two wells

The integrated interpretation of borehole images and PTS logs is presented in detail for two wells in this section and summarised for all imaged wells in Section 3.3.

In the production well at location #9 (Figure 6A), two feed zones were clearly associated with fracture clusters of high apparent thickness and seen on the travel-time image (Figure 8A-B). The fractures in the major feed zone are consistent with a fault core and its damage zone as it combines an F_FAULT fracture that truncates other fractures, and a change of acoustic amplitude above and below. This permeable fault was not previously identified from stratigraphy and 3D geological modeling. Other fractures seen on the travel-time image of similar apparent thickness occur outside of permeable zones. Conversely, no fractures were identified in other minor feed zones which suggests a contribution of matrix permeability. A striking feature in this production well is the low fracture density averaged over the entire well (0.06 fractures/metre, not corrected for orientation sampling bias). There are large intervals where >50% of the image azimuth is interpretable so this low fracture density represents the rock mass.

ISSN 2703-4275

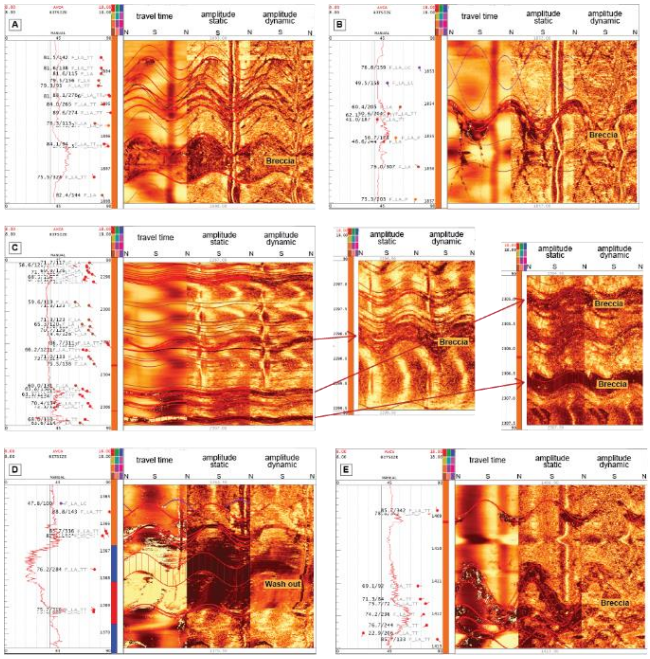

Figure 5: Examples of brecciated patterns and washout. A) Fault breccia within a feed zone (well location #10). B) Appearance of a breccia, but likely related to spalling between fractures (well location #10). C) Fault zone with multiple fault core breccias (10 m-long interval and close-ups of breccias; well location #8). D) Interval of washout in a feed zone due to dense fracturing (well location #6). The fracture with large apparent thickness (~25 cm) is likely composed of multiple, thinner fractures between which spalling from the borehole wall has occurred. E) Apparent fault breccia not related to any permeability (well location #10). From left to right on each panel: caliper calculated from the borehole image, drill bit size and feature orientation; statically normalised travel-time; statically normalised amplitude; dynamically normalised amplitude.

In the injection well at location #7 (Figure 6B), permeability is interpreted as being mostly fracture controlled. The major FZ1 includes fractures seen on the travel-time image with elevated apparent thickness, a F_FAULT feature interpreted as a micro-fault and a 2 metre-thick washout. Minor FZ2 has a 0.6 metre-thick brecciated texture zone consistent with a fault zone. Minor FZ3 has several intersecting fractures. The low fracture density (0.09 fractures/metre) between 1450 and 1940 mRF is consistent with the lack of feed zones. Conversely, the higher fracture density (0.9 fractures/metre) between 1940 and 2612 mRF does not translate into clear feed zones as defined from PTS logs, even though there are multiple fractures seen on travel-time image of elevated apparent thickness, and a F_FAULT feature.

3.3 Characteristics of fractures within and outside permeable zones: summary of all acoustic borehole images

Several permeable zones were identified in each of the eight imaged wells (Figures 7 and 8). Most permeable zones, and especially the major permeable zones, are interpreted as being structurally controlled. Indeed, most permeable zones coincide with one or several of the following characteristics:

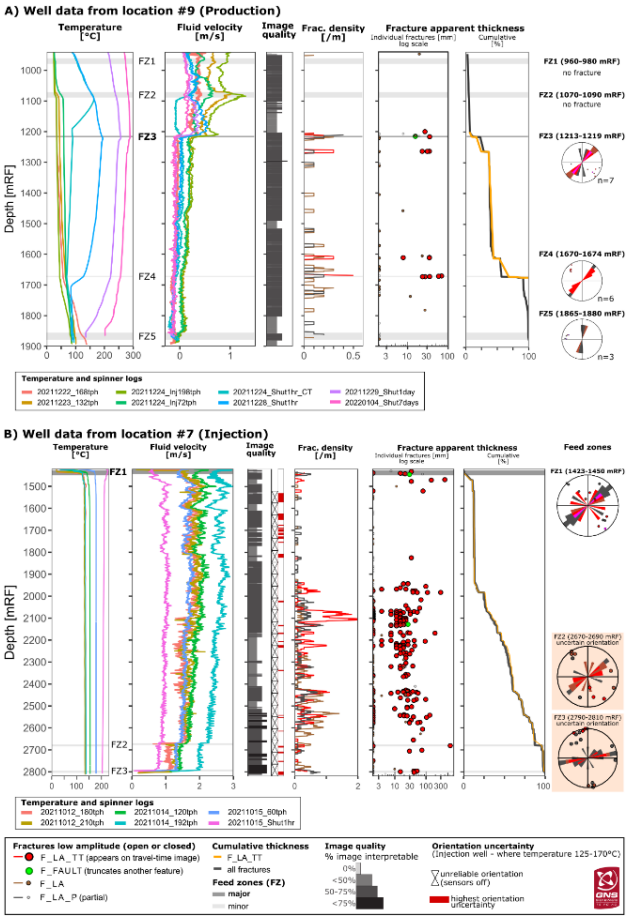

Figure 6: Integration of PTS and borehole image interpretation to reveal fracture controls on permeability. A) Production well at location #9. Major feed zone FZ3; minor feed zones FZ4 and FZ2 are shown in Figure 8A, 8B and 8D, respectively. B) Injection well at location #7 where temperature exceeded sensor rating and image was reoriented (Section 2.4).

- single fracture seen on travel-time image
- cluster of fractures seen on travel time image
- fractures of elevated apparent thickness
- a fracture that truncates another fracture (labelled "F_FAULT")
- a breccia pattern
- a series of fractures distributed over a larger interval.

Fractures in permeable zones generally have an apparent thickness at the borehole wall higher than 1 pixel (~5 mm) due to localized spalling from borehole walls within these fractures and acoustic signal scattering. Zones of washouts, i.e., where the borehole is locally enlarged over a few metres, have also been associated with major permeable zones. These washout zones are likely composed of multiple intersecting fractures that have mechanically weakened the rock and caused borehole enlargement during drilling.

However, these listed features do not guarantee permeability, as they also occur in zones where no permeability has been noted on PTS logs. For example, the high density of fractures seen on the travel time image, including some of elevated

apparent thickness, occur in the well at location #7 outside permeable zones (Figures 6-8). Another example is the brecciated pattern zone in well at location #9 that is not permeable (Figure 8E). Fractures associated with that brecciated pattern have similar orientation to those found in permeable zones in the same well so the apparent lack of permeability is probably not due to being badly oriented for reactivation (a systematic analyses of fractures' critically stressed state is beyond scope of this study).

The dominant fracture orientation across all borehole images is a NE-SW strike with high dip magnitude (75% of fractures have a dip magnitude >70°; 90% have a dip magnitude >60°), consistent with the fabric of the Taupō Rift (such as the Rotokawa Fault zone, Figure 1) and similar to that observed in the nearby Wairakei and Rotokawa geothermal fields (McNamara et al., 2015; McNamara et al., 2019). Some variations in strike orientation to N-S and E-W occur locally but there is no systematic relationship to their presence or absence in permeable zones, or to permeable zone size (Figure 7).

F_FAULT features commonly, but not always, occur in permeable zones. These features can be: 1) partial fractures stopping on another fracture as documented in schists near the Alpine Fault (Massiot et al., 2018), that could happen at Tauhara with cooling joints in welded ignimbrites; 2) isolated small faults, 3) part of fault zones that can contain multiple fault slip surfaces. Case 1) is difficult to rule out. Cases 2-3 may be related to reservoir-scale faulting and position within a damage zone. If breccia patterns, F_FAULT or clusters of fractures seen on travel-time image are indeed part of a fault's damage zone but are not in a permeable zone, the lack of permeability indicators may be attributed to sealing by hydrothermal minerals or lack of connectivity to other permeable fractures (Kissling and Massiot, 2023), at least where the borehole intersected them. During the borehole image interpretation, fractures clearly seen on travel-time images, fracture clusters and breccia patterns that have elevated potential to be permeable, are reported for further interpretation of permeability in the well as further data is collected during production. They are also considered for inclusion in the 3D geological model.

There are rare occasions where no clear fractures are identified in permeable zones, even though the image quality is sufficient to identify any occurring fractures (Figures 6, 7 and 8D). In these cases, permeability is interpreted as arising from the porosity of the formation. These permeable zones are generally minor.

Permeable zones in the study wells are distributed in depth within and across the wells and occur in several stratigraphic formations. Combined with the clear evidence of fractures for most permeable zones, this suggests that permeability in the Tauhara Geothermal Field is mainly structural rather than formational (i.e., where the connected pore space would provide pathways for fluids). Large sections of losses of circulation prevent full assessment of the effects of stratigraphy on permeability.

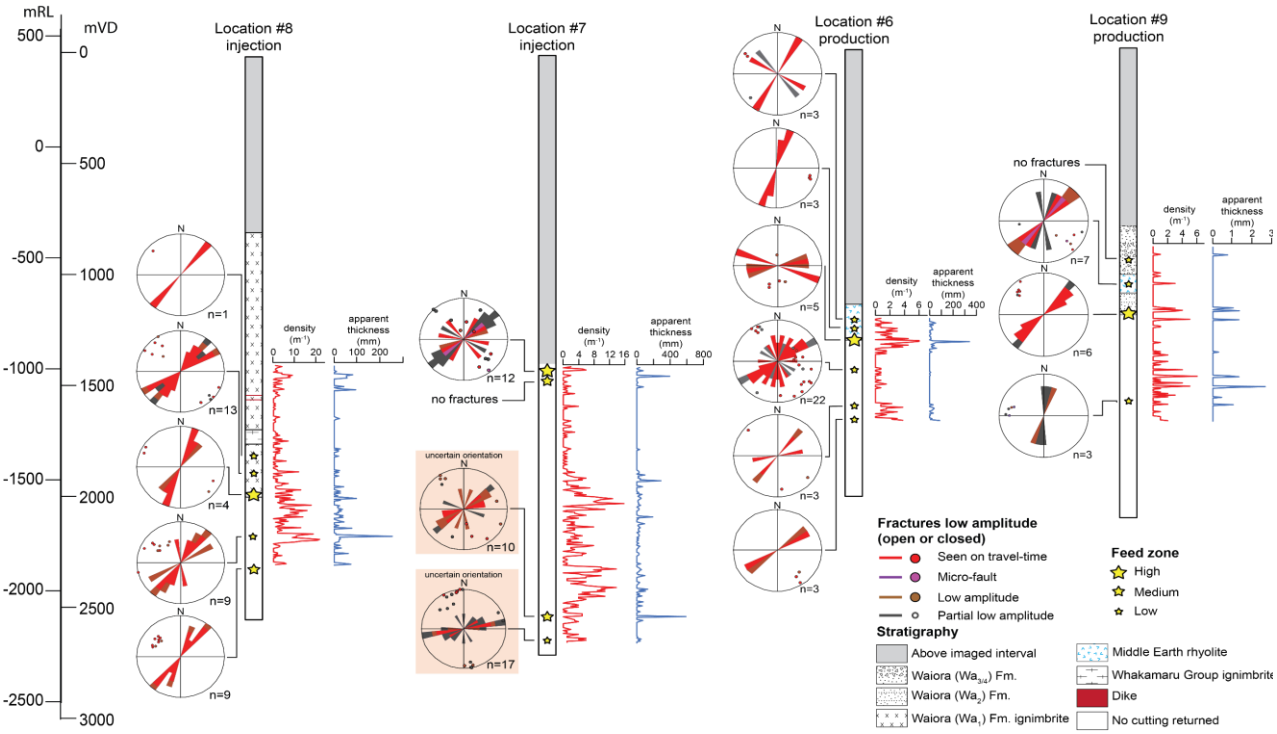

Figure 7: Correlation between permeable zones and fractures interpreted from borehole images. For each of the four boreholes, data presented are: stereonet (rose diagram and pole to planes in lower hemisphere projection) of fractures in feed zones (n is the number of fractures); stratigraphy from drill cuttings in the imaged interval and feed zones represented as stars; fracture density; apparent fracture thickness. In well at location #7 where temperature exceeded sensor rating, stereonets represent fracture orientations after re-orientation (Section 2.4) and remain uncertain. mRL: metres below sea level; mVD: metres below ground level.

ISSN 2703-4275

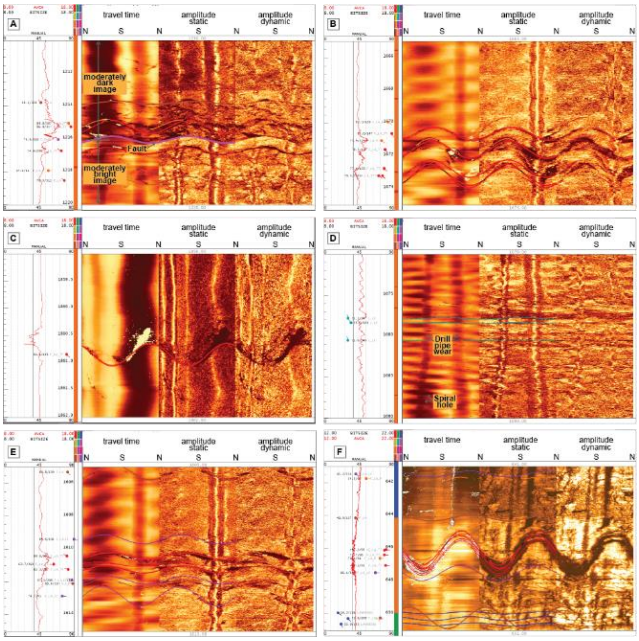

Figure 8: Examples of fractures that are good contenders for being permeable. A-D are located within feed zones; on the contrary, PTS logs in E-F show no evidence of permeability. A) Fault with a change of acoustic amplitude above and below and an image character consistent with a fault core and damage zone (well location #9). B) Cluster of F_LA_TT with a well-defined SE dip direction located in a feed zone (well location #9). C) Single

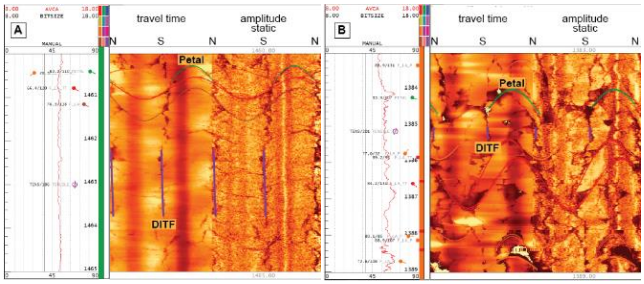

Figure 9: A) Examples of DITF and PCF features (well location #11). The oblique stress-induced straight segments were observed only in this well and in this interval. B) Complex interaction between DITF, PCF and natural fractures that required careful consideration (well location #11). Same display scheme as Figure 5.

3.4 In-situ stress feature appearance and interaction with natural fractures

Induced features form on the borehole wall during drilling as a result of the local stress field around the borehole. In vertical wells (assuming one of the principal stresses is vertical) the orientation of borehole breakouts, drilling induced tensile fractures (DITF) and petal centreline fractures (PCF) indicate the orientations of the minimum (S_{hmin}) and maximum (S_{Hmax}) horizontal stress directions (Zoback et al., 2003; Davatzes and Hickman, 2010; Massiot et al., 2015).

DITFs and PCFs are observed in all imaged wells but are more frequent in near-vertical sections (<15° from vertical). Borehole breakouts were not observed, similarly to other TVZ borehole images where only a few or none have been identified. Differentiating between natural fractures that can be partial and/or cross-cut each other, and in-situ stress features, can be difficult in sections of images (Figure 9). For this reason, DITF identification is limited to borehole-axial pairs of features opposed by 180°±10°. PCF are identified only where the combination of a partial fracture merging into two centreline fractures, i.e., borehole-axial pair of features opposed by <170°. Partial features that are not clearly associated with centrelines are labelled "partial fractures". Therefore, this "partial fracture" category can contain both natural and in-situ stress-induced fractures. This system increases confidence in features clearly labelled as in-situ stress-induced (DITF, PCF) and natural (full sinusoids) to aid with structural permeability assessment.

4. DISCUSSION AND CONCLUSIONS

A high borehole image acquisition rate was achieved (82% of open-hole sections) for the post-2019 acoustic borehole images of the Tauhara Geothermal Drilling Program. This high rate was achieved despite the reservoir temperature (250°C- >300°C) exceeding the ABI43 tool rating (170°C). Intervals where logging temperature exceeded the orientation sensor (125°C) still provided valuable information on the occurrence and appearance of fractures. For the well at location #7 where only 7% of the imaged interval was oriented due to a shallow hot inflow, image re-orientation using drill-pipe wear provided additional indication of fracture orientation, though with high uncertainties.

Borehole image interpretation was valuable throughout the drilling campaign for well targeting, and this value was maximized by providing time for data interpretation and input into the drilling program. Completion testing (specifically, interpretation of feed zones based on PTS data) guided areas of interest for borehole image interpretation and borehole image interpretations allowed refinement of feed zone intervals defined from PTS. Occasionally, identification of clear fractures on the borehole image supported the delineation of small permeable zones where PTS signals alone would have been insufficient. The dominant high fracture dip magnitude (largely >70°) reinforced the decision to design and drill deviated wells with high inclination (>20°) at target zones, to increase probability of intersecting more fractures and/or faults and their damage zones. Integrated interpretation of borehole images, PTS logs and stratigraphy from drill cuttings helped with fine tuning well design parameters such as kick-off depth, inclination at target and target depth of subsequent wells for increased chance of intersecting known regions of enhanced permeability. Replacing consecutive drilling in multiple-well pads by alternated drilling between well pads (one well per pad at any time) also provided an opportunity for timely acquisition and integration of all available data into an adaptive drilling program.

A major outcome of borehole imaging at the Tauhara Geothermal Field has been the shift of the conceptual model from matrix-dominated permeability towards a hybrid model of matrix and fracture permeability. This concept is based on the key fact that most large permeable zones were found to

be correlated with fractures, fractured zones or faults (defined by high fracture aperture and/or fracture density, and/or specific fracture appearance). These findings need to be reconciled with the well documented pressure communication across Wairakei-Tauhara.

Geological faults were inferred from the new borehole images using indicators including breccia textures, clusters of thick fractures seen on travel time images, presence of F_FAULT feature, and change of acoustic amplitude. These fault indicators defined from borehole images have been used in combination with available knowledge of stratigraphic offsets, active faults mapped on surface and geophysical surveys (e.g., magnetotelluric, gravity), to further refine the Tauhara 3-D geological model. Borehole imaging supports identification of faults (or fault segments) that 1) may have smaller displacement than deemed significant based on stratigraphic offsets alone, or 2) occur within thick formations. Borehole images also provide information over large intervals that lack cuttings due to total losses of drilling fluid circulation (Figure 7). While acoustic images are not as powerful as resistivity images to identify changes in lithologies, it is expected that major lithology changes (e.g., from ignimbrites to the metamorphic basement) would have been detected on acoustic images. Borehole imaging thus supported revising the 3-D geological model during and after the drilling campaign.

In-situ stress features rarely occurred in the Tauhara borehole images compared to other borehole images acquired within the adjacent Te Mihi region of the nearby Wairakei Geothermal Field (McNamara et al., 2019). Further studies are required to explain this observation.

Future quantitative analysis of permeable zones and fracture characteristics (orientation, density, thickness) in relation to the in-situ stress regime, fault network and potential mechanical stratigraphy (with some horizons that may be consistently more fractured than other) will support management of the Tauhara Geothermal Field. Exploring why some breccia textures and fractures that are good contenders to be permeable but do not coincide with permeable zones defined from PTS will further the understanding of the geothermal reservoir and regional tectonics.

REFERENCES

Barton, C.A., Zoback, M.D. (1992). Self-similar distribution and properties of macroscopic fractures at depth in crystalline rock in the Cajon Pass scientific drill hole, *Journal of Geophysical Research*, **97**, 5181–5200.

Davatzes, N.C., and Hickman, S.H. (2010). Stress, fracture, and fluid-flow analysis using acoustic and electrical image logs in hot fractured granites of the Coso geothermal field, California, USA, In: Pöppelreiter, M., García-Carballido, C., and Kraaijveld, M. (editors): Dipmeter and Borehole Image Log Technology, *American Association of Petroleum Geologists Memoir*, **92,** 259-293.

Genter, A., Castaing, C., Dezayes, C., Tenzer, H., Traineau, H., Villemin, T. (1997). Comparative analysis of direct (core) and indirect (borehole imaging tools) collection of fracture data in the Hot Dry Rock Soultz reservoir (France), *Journal of Geophysical Research,* **102**, 15419-15431.

Halwa, L., Wallis, I.C., Lozada, G.T. (2013). Geological analysis of the volcanic subsurface using borehole resistivity images in the Ngatamariki Geothermal Field, New Zealand, *Proceedings*, 35th New Zealand Geothermal Workshop, Rotorua, New Zealand.

Hansen, B., Buczak, J. (2010). Making interpretable images from image logs, In: Pöppelreiter, M., García-Carballido, C., and Kraaijveld, M. (editors): Dipmeter and Borehole Image Log Technology, *American Association of Petroleum Geologists Memoir*, **92,** 51-66.

Jolie, E., Scott, S., Faulds, J., Chambefort, I., Axelsson, G., Gutiérrez-Negrín, L.C., Regenspurg, S., Ziegler, M., Ayling, B., Richter, A., Zemedkun, M.T. (2021). Geological controls on geothermal resources for power generation, *Nature Reviews Earth & Environment*, **2**, 324-339.

Kissling, W.M., Massiot, C. (2023). Modelling of flow through naturally fractured geothermal reservoirs, Taupō Volcanic Zone, New Zealand. *Geothermal Energy*, **11(1)**, p.20.

Lofts, J., Bourke, L.T. (1999). The recognition of artefacts from acoustic and resistivity borehole imaging devices, *Geological Society Special Publications* **159**, 59-76.

Masri, A., Barton, C.A., Hartley, L., Ramadhan, Y. (2015). Structural Permeability Assessment Using Geological Structural Model Integrated with 3D Geomechanical Study and Discrete Facture Network Model in Wayang Windu Geothermal, *Proceedings*, 40th Workshop on Geothermal Reservoir Engineering, Stanford University, California, USA.

Massiot, C., McNamara, D.D., Lewis, B. (2015). Processing and analysis of high temperature geothermal acoustic borehole image logs in the Taupo Volcanic Zone, New Zealand, *Geothermics*, **53**, 190-201.

Massiot, C., McLean, K., McNamara, D.D., Sepulveda, F., Milicich, S.D. (2017a). Discussion between a reservoir engineer and a geologist: Permeability identification from completion test data and borehole image logs integration, *Proceedings*, 39th New Zealand Geothermal Workshop, University of Auckland, Auckland, New Zealand.

Massiot, C., Nicol, A., McNamara, D.D., Townend, J. (2017b). Evidence for tectonic, lithologic, and thermal controls on fracture system geometries in an andesitic high-temperature geothermal field, *Journal of Geophysical Research: Solid Earth*, **122**, 6853-6874.

Massiot, C., Célérier, B., Doan, M-L., Little, T.A., Townend, J., McNamara, D.D., Williams, J., Schmitt, D.R., Toy, V.G., Sutherland, R., et al. (2018). The Alpine Fault hanging wall viewed from within: structural analysis of ultrasonic image logs in the DFDP-2B borehole, New Zealand, *Geochemistry, Geophysics, Geosystems*, **19**, 2492-2515.

Massiot, C., McNamara, D.D., Milicich, S.D., Villamor, P., Mclean, K., Sepulveda, F., Ries, W.F. (2020). Fracture Permeability in a Pervasively Fractured Rock Mass: the role of Regional Tectonics at Te Mihi, Wairakei Geothermal Field, New Zealand, *Proceedings*, World

ISSN 2703-4275

Geothermal Congress 2020+1, Harpa Conference Centre and online, Reykjavik, Iceland.

McDowell, J., Bixley, P., Sepulveda, F. (2020). Conceptual Model Evolution of the Tauhara Geothermal Reservoir from 1960-2020, *Proceedings*, World Geothermal Congress 2020+1, Harpa Conference Centre and online, Reykjavik, Iceland.

McNamara, D.D., Massiot, C., Lewis, B., Wallis, I.C. (2015). Heterogeneity of structure and stress in the Rotokawa Geothermal Field, New Zealand, *Journal of Geophysical Research*, **120**, 1243-1262.

McNamara, D.D., Milicich, S.D., Massiot, C., Villamor, P., McLean, K., Sépulveda, F., Ries, W.F. (2019). Tectonic controls on Taupo Volcanic Zone geothermal expression: insights from Te Mihi, Wairakei Geothermal Field, *Tectonics*, **38**, 3011-3033.

Milicich, S.D., Massiot, C., Lawrence, M.J.F. (2021). Tauhara Geothermal Field – interpretation of the borehole image in well TH30, *GNS Science Consultancy Report 2021/49*, 25 p.

Millett, J.M., Planke, S., Kästner, F., Blischke, A., Hersir, G.P., Halldórsdóttir, S., Flóvenz, Ó.G., Árnadóttir, S., Helgadóttir, H.M., Vakulenko, S., Buryak, S., et al. (2020). Sub-surface geology and velocity structure of the Krafla high temperature geothermal field, Iceland: Integrated ditch cuttings, wireline and zero offset vertical seismic profile analysis, *Journal of Volcanology and Geothermal Research*, **391**, 106342.

Mutonga, M., Fujimitsu, Y. (2021). An insight of the subsurface through borehole images - case study of MW-34 Menengai Geothermal Field, Kenya, *Proceedings*, 43rd New Zealand Geothermal Workshop, held online, New Zealand.

New Zealand Active Faults Database. 2003–. www.gns.cri.nz/Home/Products/Databases/Active-Faults-Database-of-New-Zealand. [updated 2020 Oct 20; accessed 2022 September]

Poppelreiter, M., Garcia-Carballido, C., Kraaijveld, M. (2010). Borehole image log technology: application across the exploration and production life cycle, In: Pöppelreiter, M., García-Carballido, C., and Kraaijveld, M. (editors): Dipmeter and Borehole Image Log Technology, *American Association of Petroleum Geologists Memoir*, **92,** 1-13.

Rider, M.H. (1996). The geological interpretation of well logs, 2nd edition, Whittles Publishing, Caithness, Great Britain, 280 p.

Risk, G.F., Rayner, H.H., Stagpoole, V.M., Graham, D.J., Dawson, G.B. Bennie, S.L. (1984). Electrical resistivity survey of the Wairakei geothermal field. *Report-Geophysics Division*, **200**.

Rosenberg MD, Wilson CJN, Bignall G, Ireland TR, Sepulveda F, Charlier BLA. (2020). Structure and evolution of the Wairakei–Tauhara geothermal system (Taupo Volcanic Zone, New Zealand) revisited with a new zircon geochronology. *Journal of Volcanology and Geothermal Research.* 390:106705.

Rowland, J.V. Sibson, R.H. (2001). Extensional fault kinematics within the Taupo Volcanic Zone, New Zealand: Soft-linked segmentation of a continental rift system. *New Zealand Journal of Geology and Geophysics*, **44(2)**, 271-283.

Vidal, J., Genter, A. (2018). Overview of naturally permeable fractured reservoirs in the central and southern Upper Rhine Graben: Insights from geothermal wells, *Geothermics*, **74**, 57-73.

Villamor, P., Berryman, K.R., Ellis, S.M., Schreurs, G., Wallace, L.M., Leonard, G.S., Langridge, R.M., Ries, W.F. (2017). Rapid Evolution of Subduction-Related Continental Intraarc Rifts: The Taupo Rift, New Zealand, *Tectonics*, **36(10)**, 2250-2272.

Wallis, I.C., McNamara, D., Rowland, J.V. Massiot, C. (2012). The nature of fracture permeability in the basement greywacke at Kawerau Geothermal Field, New Zealand, *Proceedings*, 37th Workshop on Geothermal Reservoir Engineering, Stanford University, California, USA.

Zemanek, J., Glenn, E.E., Norton, L.J., Caldwell, R.L. (1970). Formation evaluation by inspection with the borehole televiewer, *Geophysics*, **35**, 254-269.

Zoback, M.D., Barton, C.A., Brudy, M., Castillo, D.A., Finkbeiner, T., Grollimund, B.R., Moos, D.B., Peska, P., Ward, C.D., Wiprut, D.J. (2003). Determination of stress orientation and magnitude in deep wells, *International Journal of Rock Mechanics and Mining Sciences*, **40**, 1049-1076.

ISSN 2703-4275